


Inducing aortic aneurysm/dissection in zebrafish: evaluating the efficacy of β -Aminopropionic Nitrile as a model

Jiarui Zhang ^{a,b,†}, Yaowen Liang ^{b,c,†}, Weiyue Zeng ^{a,b,†}, Xiaoyan Gao ^{a,b}, Dingchen Wang ^{a,b},
Cong Mai ^{a,b}, Zhuoheng Lin^b, Haishan Zhao ^b and Xin Li ^b

^aSchool of Medicine, South China University of Technology, Guangzhou, People's Republic of China; ^bDepartment of Emergency Medicine, Guangdong Provincial People's Hospital (Guangdong Academy of Medical Sciences), Southern Medical University, Guangzhou, People's Republic of China; ^cShantou University Medical College, Shantou, People's Republic of China

ABSTRACT

Aortic aneurysm/dissection (AAD) poses a life-threatening cardiovascular emergency with complex mechanisms and a notably high mortality rate. Zebrafish (*Danio rerio*) serve as valuable models for AAD due to the conservation of their three-layered arterial structure and genome with that of humans. However, the existing studies have predominantly focused on larval zebrafish, leaving a gap in our understanding of adult zebrafish. In this study, we utilized β -Aminopropionic Nitrile (BAPN) impregnation to induce AAD in both larval and adult zebrafish. Following induction, larval zebrafish exhibited a 28% widening of the dorsal aortic diameter ($p < 0.0004$, $n = 10$) and aortic arch malformations, with a high malformation rate of 75% (6/8). Conversely, adult zebrafish showed a 41.67% (5/12) mortality rate 22 days post-induction. At this time point, the dorsal aortic area had expanded by 2.46 times ($p < 0.009$), and the vessel wall demonstrated significant thickening ($8.22 \pm 2.23 \mu\text{m}$ vs. $26.38 \pm 10.74 \mu\text{m}$, $p < 0.05$). Pathological analysis revealed disruptions in the smooth muscle layer, contributing to a 58.33% aneurysm rate. Moreover, the expression levels of *acta2*, *tagln*, *cnn1a*, and *cnn1b* were decreased, indicating a weakened contractile phenotype. Transcriptome sequencing showed a significant overlap between the molecular features of zebrafish tissues post-BAPN treatment and those of AAD patients. Our findings present a straightforward and practical method for generating AAD models in both larval and adult zebrafish using BAPN.

ARTICLE HISTORY

Received 27 November 2023
Revised 23 January 2024
Accepted 17 February 2024

KEYWORDS

Aortic aneurysm/dissection (AAD); Zebrafish; β -Aminopropionic Nitrile (BAPN); Animal model

Summary: The AAD model of zebrafish was successfully established by employing BAPN. This model provides a fundamental basis for exploring AAD-associated metabolites and conducting gene screening.


1. Introduction

Aortic Aneurysm/Dissection (AAD) is a critical cardiovascular emergency characterized by a bulge in the aortic wall or a tear in the innermost layer of the aorta. A combination of aortic wall stress and abnormalities of the medial layer of the aortic wall leads to disruption of the media and an intimal tear with subsequent penetration of blood, which splits the aortic wall layers to form a true-false lumen. AAD is relatively rare, with an

estimated incidence of up to 35 cases per 100,000 people. It primarily affects individuals aged between 65 and 70 years (Kim and Stansfield 2017; Lin et al. 2023). However, the mortality rate associated with AAD is extremely high, especially if definitive treatment is delayed, and is estimated to cause 2,000, 000 deaths annually (Powell and Brady 2004; Nienaber et al. 2016). Despite the severity, effective pharmacologic interventions or therapeutic strategies for AAD are still lacking. Currently, surgery is the only treatment for AAD, indicated for large asymptomatic, symptomatic, or ruptured aneurysms due to the rapid progression of the disease, the complexity of surgery, and the large number of post-operative complications (Jingjing Li et al. 2018; Yang et al. 2020). There is an urgent need to comprehensively

CONTACT Xin Li  sylixin@scut.edu.cn  Department of Emergency Medicine, Guangdong Provincial People's Hospital (Guangdong Academy of Medical Sciences), Southern Medical University, Guangzhou, Guangdong, People's Republic of China, 510180; Haishan Zhao  zhaohaishan@gdph.org.cn  Department of Emergency Medicine, Guangdong Provincial People's Hospital (Guangdong Academy of Medical Sciences), Southern Medical University, Guangzhou, Guangdong, People's Republic of China, 510180; Zhuoheng Lin  linzhuoh@163.com  Department of Emergency Medicine, Guangdong Provincial People's Hospital (Guangdong Academy of Medical Sciences), Southern Medical University, Guangzhou, Guangdong, People's Republic of China, 510180.

[†]Jiarui Zhang, Yaowen Liang and Weiyue Zeng contributed equally to this work.

 Supplemental data for this article can be accessed online at <https://doi.org/10.1080/19768354.2024.2322055>.

© 2024 The Author(s). Published by Informa UK Limited, trading as Taylor & Francis Group
This is an Open Access article distributed under the terms of the Creative Commons Attribution-NonCommercial License (<http://creativecommons.org/licenses/by-nc/4.0/>), which permits unrestricted non-commercial use, distribution, and reproduction in any medium, provided the original work is properly cited. The terms on which this article has been published allow the posting of the Accepted Manuscript in a repository by the author(s) or with their consent.

investigate the underlying mechanisms and identify new therapeutic targets. This underscores the importance of using animal models, instead of patients, to simulate the disease and explore its mechanisms and potential treatments (Andrew Prendergast et al. 2022).

Considering that the cardiovascular system of zebrafish (*Danio rerio*) exhibits similarity to that of mammals in both anatomical structure and physiological function (Konstantin Stoletov et al. 2009; Jichun Bahrami and Childs 2020; Han et al. 2021), zebrafish have become extensively employed in cardiovascular disease research (Peterson and Macrae 2012; Philipp Gut et al. 2017). The three-layered arterial structure, consisting of an intima, a midmembrane, and an epithelium, is similar to that of humans (Marie Hoareau et al. 2022). Additionally, with a genome that is approximately 87% conserved compared to humans, zebrafish proves to be a suitable model for studying the pathogenesis of AAD. Abrial et al. demonstrated that deficiency of *Itbp1* and *Itbp3* in zebrafish larvae resulted in an increase in the diameter of the outflow tract (OFT), indicating a marfan like phenotype of aortic aneurysm widening (Marine Abrial et al. 2022). Kuang et al. demonstrated that knocking down *FOXE3* in zebrafish larvae can lead to aortic arch malformation, which can reflect ascending aortic aneurysm in mice (Shao Qing Kuang et al. 2016). Transient overexpression of *SMAD3a* in zebrafish embryos induced aneurysms, indicated by an enlarged dorsal aorta diameter (Mary B Sheppard et al. 2023).

These literature established methods for assessing aneurysm occurrence. However, artificially modifying the expression of specific genes involved in the disease only replicates a fraction of the pathogenesis observed in patients, limiting its universality. Moreover, all current articles on AAD modeling using zebrafish have focused on larval individuals, failing to fully capture the clinical features of AAD occurrence in adult patients.

BAPN is a chemical inhibitor that targets lysyl oxidase (LOX) and has been widely utilized to induce aortopathy including AAD in multiple species (Tongyun Chen et al. 2021; Hai-Qiong Zheng et al., 2020; Alexander H Shannon et al. 2019). It is proposed that BAPN disrupts aortic integrity by inhibiting the formation of desmosine, which is catalyzed by LOX to crosslink the lysine residue in extracellular matrix proteins such as elastin and collagens (Levene 1962). Inhibition of this process by BAPN could lead to structural changes in the extracellular matrix, contributing to the development of aortopathy.

In the current study, we established an animal model of AAD using both larval and adult zebrafish induced by BAPN. We used Tg[flk:eGFP] zebrafish, in which eGFP is

driven by an endothelial-specific promoter, to visualize the vascular system under fluorescence microscopes and validate the feasibility of AAD modeling. Disruptions in the smooth muscle layer revealed by pathological analysis, along with changes in the molecular signature, further confirm an AAD-like transition in the adult zebrafish model induced by BAPN. Our findings provide a robust method to generate AAD model in adult zebrafish.

2. Result

2.1 BAPN induced dorsal aortic widening and aortic arch deformity in larval zebrafish

To determine whether BAPN could be used as a modeling method for AAD in zebrafish, larval zebrafish of the Tg[flk:eGFP] strain were chosen for the intervention. The widening and deformity of the dorsal aorta and the aortic arch were used as evaluation indicators (Marine Abrial et al. 2022; Shao Qing Kuang et al. 2016; Mary B Sheppard et al. 2023). We administered various concentrations of BAPN to zebrafish at different developmental stages (24 hpf-7 dpf), and observed the diameter of dorsal aortic within the first five internodal vessels at the ejaculatory orifice by fluorescence microscopy (Figure 1B). Notably, the dorsal aortic diameters were significantly widened in the BAPN group compared to the controls at any time period ($P < 0.05$). The dorsal aortic diameter was significantly wider at 3 dpf than at 5 and 7 dpf. This is due to the fact that, as the zebrafish vasculature develops, the structural remodeling of the aortic wall at 4 dpf results in the emergence of a smooth muscle layer and elastic fibers. This constriction of the vasculature, shown in Figure 1A, is in line with the zebrafish vasculature's developmental process. The constriction also affects diameter observations in our study, so the time of observing the diameter of the dorsal aorta was standardized to 3 dpf. We then chose a BAPN concentration of 50 μM for the subsequent observations, considering that (1) BAPN-induced changes in aortic diameter showed the most significant difference compared to controls at this concentration (Figure 1B; $p < 0.05$); (2) The dorsal aorta showed no significant abnormal changes; (3) BAPN induced fibrous tissue-like mass and chordomorphic malformations in zebrafish, with the occurrence exceeding 50% at the concentration higher than 50 μM (Figure 1C).

After BAPN 50 μM induction for 3 dpf, dorsal aortic diameter were widened by 28% ($p < 0.0004$, $n = 10$) compared to controls and 75% (6/8) of the aortic arches were altered with malformations (Figure 1E and F), revealed an AAD-like alterations occurred in larvae zebrafish after BAPN induction.

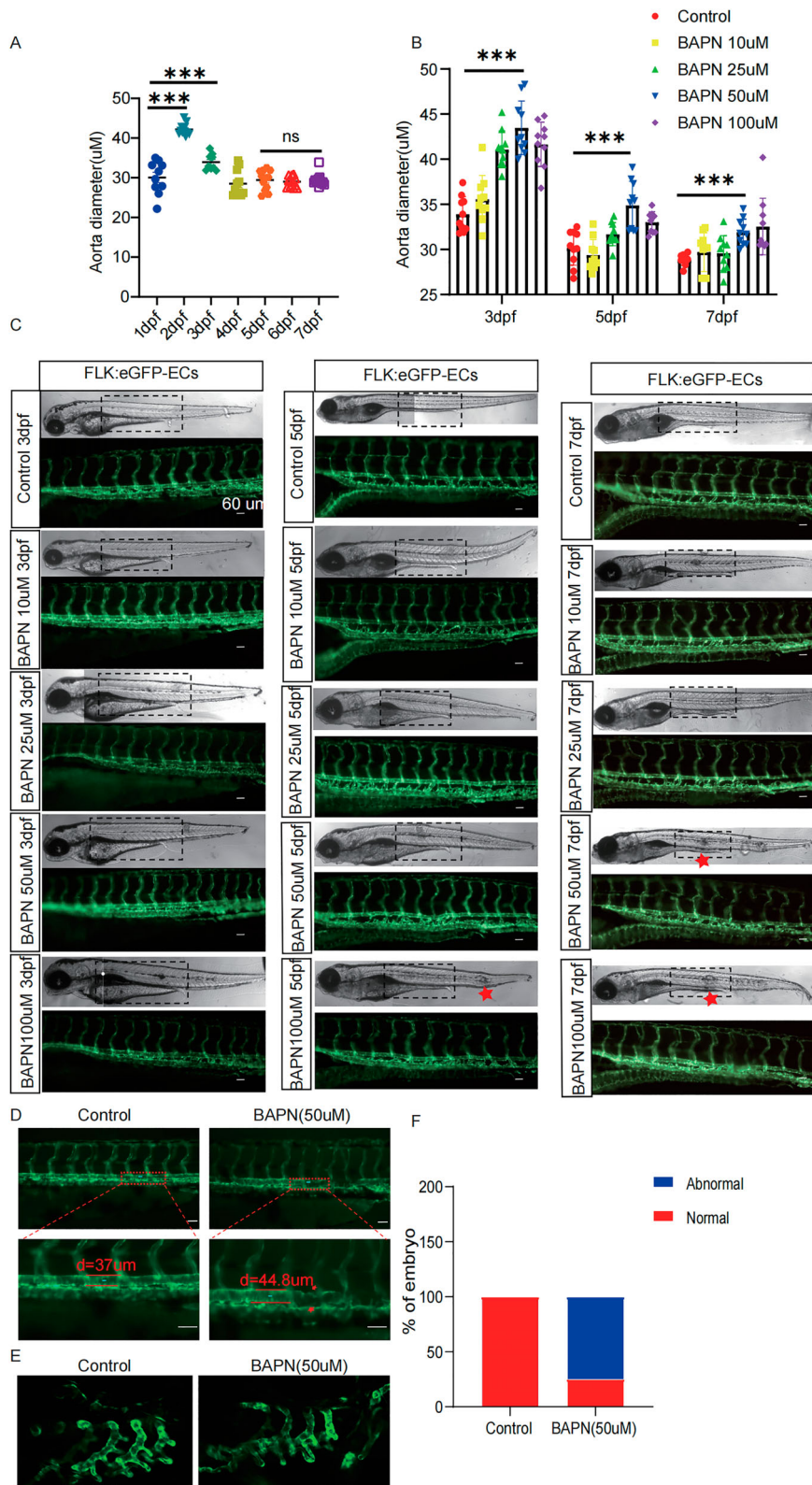


Figure 1. BAPN induced dorsal aortic widening and aortic arch deformity in larval zebrafish. **A**, statistical analysis of the diameter of the dorsal aorta of Tg[flk:eGFP] zebrafish with a sample size of $n = 10$ and a significant difference of $*** < 0.001$. **B** and **C**, statistical analysis of the dorsal aortic diameter in response to four different concentrations of BAPN, and the control groups on the 3rd, 5th, and 7th days post-treatment. The scale bars indicate a magnification of $60 \mu\text{m}$ (10x), with a sample size of $n = 10$. Statistical significance is denoted as $* < 0.05$, $** < 0.001$, and $*** < 0.0001$. **D**, Blood vessel abnormalities following BAPN administration, revealing the presence of fibrous tissue-like mass in the zebrafish body. In the present study, figure **E** shows the zebrafish control group and the group treated with BAPN under a confocal focus of $50 \mu\text{m}$. These results indicated that the administration of BAPN led to the deformation of the aortic arch. Furthermore, the statistical graph **F** displays the observed malformation of the aortic arch in diagram **E**, with a sample size of $n = 8$.

2.2 BAPN induced AAD-related pathological changes in adult zebrafish

To address the limitations of incomplete vascular development in larval zebrafish and the inability to accurately replicate the manifestations of aneurysm patients, adult zebrafish were selected as experimental subjects. We submerged adult zebrafish into different concentration gradients of BAPN (0, 0.25, 0.5, 1, 2, and 4 mM) with six fishes in each group. High concentration of BAPN, 4 and 2 mM, killed all the zebrafish at day 5 and day 18, respectively. At day 22, two and one zebrafish died in the 2 and 1 mM groups, respectively. All the fishes were survival in the 0.25 mM and the control groups (Figure S2). The dorsal aortic section and following pathological analysis revealed that vascular injury occurred only in high concentration of BAPN (1 mM 2/6; 2 mM 1/6; 4 mM 1/6). We thus chose a BAPN concentration of 1 mM and a period of 22 days for the administration.

At the time of enrollment, zebrafish were completely randomized and the starting weight and length were counted, and there was no difference between the control group [(0.44 ± 0.06 g), (3.54 ± 0.28 cm), $n = 10$] and the modeling group [(0.44 ± 0.06 g), (3.55 ± 0.27 cm), $n = 12$]. Notably, the mortality rate in the BAPN group was 41.67% (5/12; Figure 2A) within 22 days. At day 22, the weight and length of the model group were [(0.48 ± 0.07 g), (3.80 ± 0.19 cm)], which were reduced but not statistically significant ($P > 0.05$) compared to the control group [(0.52 ± 0.09 g), (3.77 ± 0.19 cm)]. As we expected, the model group developed ruptured blood vessel hemorrhage and spinal cord malformation after drug administration, with a hemorrhage rate of 58.33% (7/12) and a malformation rate of 66.7% (8/12; Figure 2B). Further, ultrasonography results showed that the dorsal aorta in the model group showed significant widening at specific locations compared to the control group (Figure S1B).

Pathological analysis revealed that a 2.46-fold enlargement in the area of the vascular lumen in the modeling group compared to the control group ($p < 0.05$; Figure 2E). In the BAPN group, the vascular structure is disrupted and vascular wall was markedly thickened (8.22 ± 2.23 μM vs. 26.38 ± 10.74 μM, $p < 0.05$; Figure 2F). Masson staining showed rupture of the smooth muscle layer at the site of vascular tear, resulting in a reduction in the thickness of the smooth muscle layer (Figure 2C). Toluidine blue staining showed disruption and degradation of the elastic lamina caused by BAPN (Figure 2G and H). As summary in Table S1, the incidence of AAD-related pathological changes in the BAPN group was 58.33% (7/12; Figure 2D) compared to that of the control group (0/10). Taken together, our results

demonstrated that in this condition, BAPN efficiently induced AAD model in adult zebrafish.

2.3 Molecular signature of BAPN-induced AAD model in adult zebrafish

We demonstrated AAD-related pathological changes in BAPN-induced zebrafish. To look into the changes in molecular level, we dissected the dorsal aorta, aortic arch for quantitative PCR. Contractile markers of SMCs, such as *acta2*, *tagln*, *cnn1a*, and *cnn1b* were significantly decreased (Figure 3A). Further, RNA sequencing identified a total of 6249 differentially expressed genes (DEGs), of which 2727 were significantly upregulated and 3208 were significantly downregulated (filtered based on standard P values < 0.05 and absolute multiples > 2 ; Figure 3B and C). KEGG analysis showed that the most significantly enriched pathways for upregulated genes included 'cytokine-cytokine receptor interactions,' followed by inflammatory cell differentiation and enrichment (Figure 3D). The top down-regulated genes were 'oxidative phosphorylation' and 'citric acid cycle (TCA cycle)' (Figure 3E), suggesting that BAPN-induced abnormalities in mitochondrial metabolism lead to AAD in adult zebrafish overlap with the pathway in human patients (Figure 3E; Erik Biros et al. 2014). Similarly, GSEA analysis revealed a SMC phenotype transition from contractile to synthetic phenotype (Figure 3G), underlying the mechanism of AAD pathogenesis. Interestingly, an enrichment of processes 'citric acid cycle and respiratory electron transport' in downregulated genes (Figure 3F) was also found, suggested the metabolic reprogramming during AAD development. We further conducted a cross analysis between our zebrafish dataset and previously published data on abdominal aortic aneurysm patients (GSE226492; Figure S3A), suggested a significant overlap of the differentially expressed genes (Figure S3C). The results were subjected to reactome enrichment analysis, which enriched a large number of pathways similar to zebrafish, such as 'Smooth Muscle Contraction,' 'Cytokine Signaling in Immune System,' and 'TCA Cycle and Respiratory Electron Transport' (Figure S3D). These results confirmed again the AAD-like transition in BAPN induced zebrafish in the molecular level.

3. Discussion

AAO has a prevalence of up to 35 per 100,000 in people aged 65–70 years, with a high mortality rate after the onset of the disease. However, there is a lack of effective drug strategies to prevent and treat AAD (Lin et al. 2023; Yihong Zhou et al. 2024). The in-depth study of the disease mechanism is inevitably inseparable

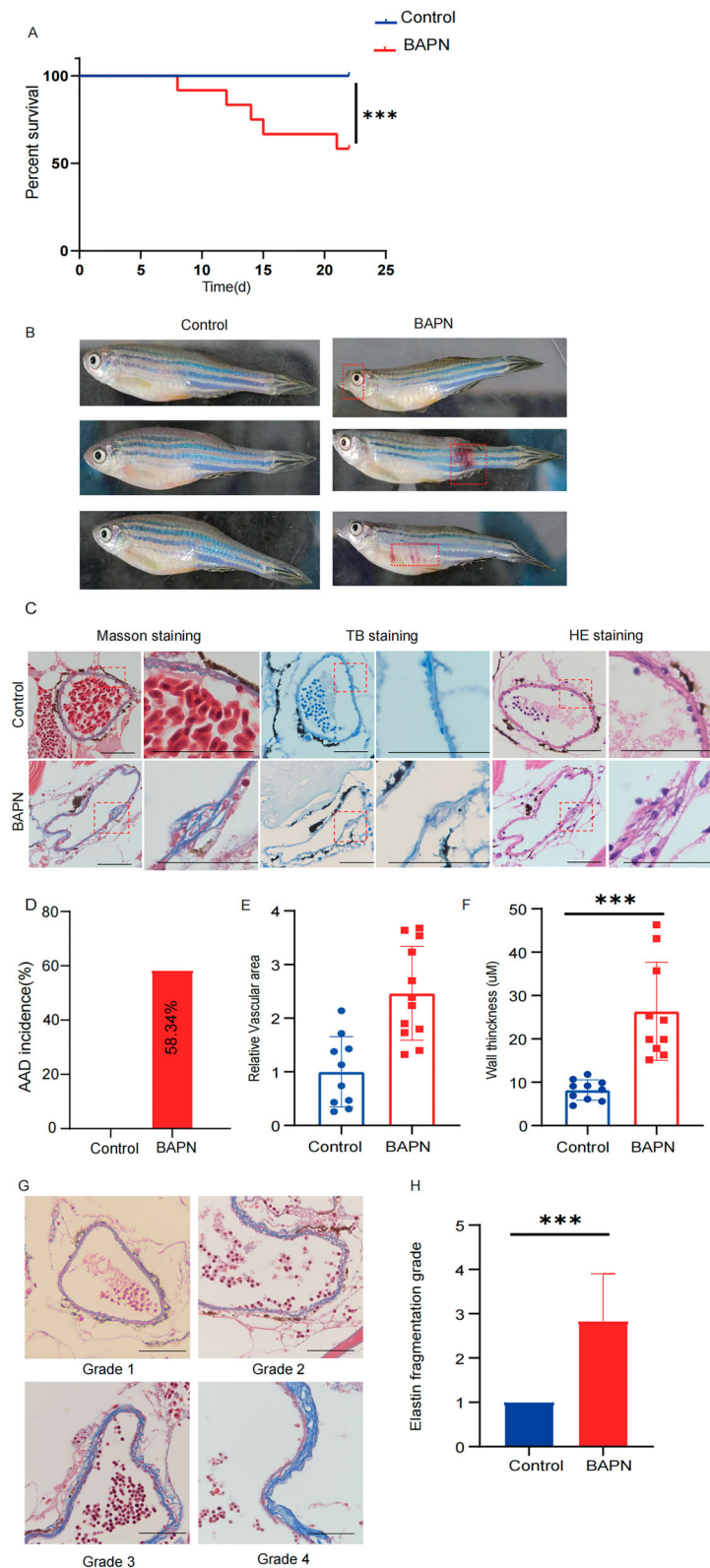


Figure 2. BAPN induced AAD-related pathological changes in adult zebrafish. **A**, the survival rate of the zebrafish during the 22-day administration period is presented through statistical analysis and a significant difference of $*** < 0.001$. **B**, a notable distinction can be observed between the zebrafish group administered with BAPN and the control group on the 22nd day after three months of treatment. It is evident that the treatment of BAPN leads to the occurrence of multiple blood vessel bleedings in the body and abnormal changes in the development of the notochord. **C**, the differences observed after the administration of BAPN are depicted in the masson, TB, and HE stained sections. The scale bars in the images represent a measurement of $100 \mu\text{m}$ ($100 \times$). **D**, based on the pathological changes of zebrafish dorsal aorta, the incidence of AAD after treatment of zebrafish BAPN was statistically analyzed, $n = 12$; **E** and **F**, statistics of relative area and wall thickness of blood vessels in pathological sections; **G** and **H**, elastin staining showed fragmentation grades. Grading keys are shown on the left ($p < 0.05$), Scale bars: $100 \mu\text{m}$ ($100 \times$). Data are presented as mean \pm SEM. $*p < 0.05$.

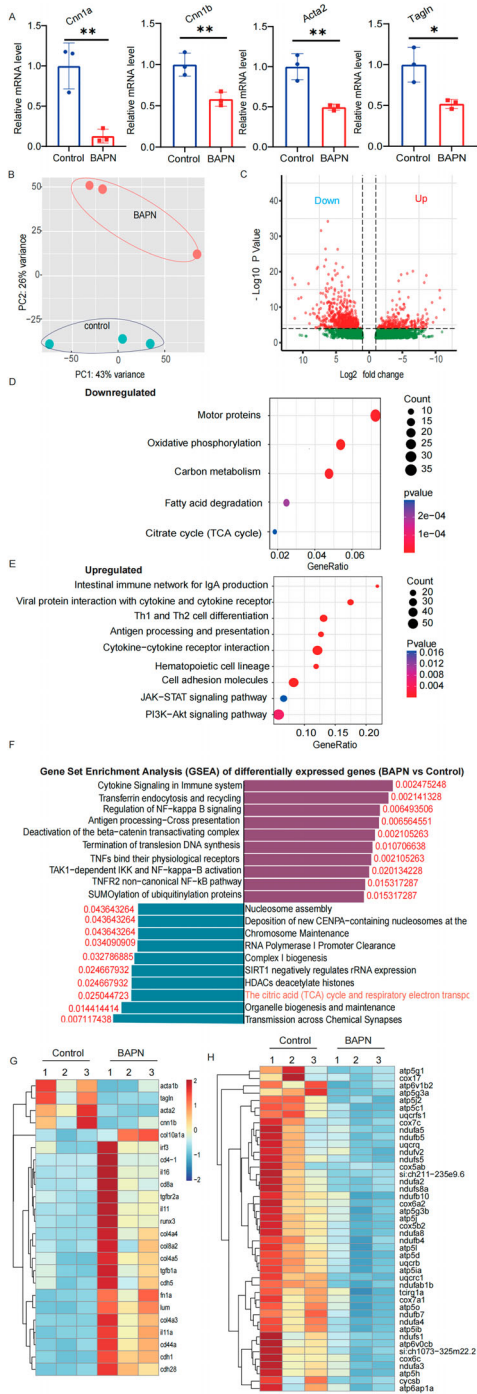


Figure 3. Verification of molecular mechanisms after immersion in BAPN induction in adult zebrafish. **A**, exhibits a histogram illustrating the relative expression levels of CNN1a, CNN1b, ACTA2, and TAGLN in control and BAPN-treated zebrafish, as determined by qPCR. Statistical significance was assessed using an unpaired t-test, with a sample size of 3 zebrafish per group and a total of three groups ($*P < 0.05$; $**P < 0.01$). **B**, Principal component (PC) analysis. **C**, presents a volcano plot illustrating all the differentially expressed genes (DEGs). **D** and **E**, KEGG pathway enrichment analyses for up- and downregulated differentially expressed genes (DEGs). **F**, encompassed Reactome Gene Set Enrichment Analysis (GSEA), with a cut-off p -value set at 0.05. Heatmap for DEGs annotated as **(G)** 'smooth muscle phenotypic transformation' and **(H)** 'oxidative phosphorylation' in the KEGG database.

from animal models. In this study, we developed a robust way to establish zebrafish AAD models. We demonstrated that the BAPN infiltration method can model AAD in larvae as well as adult zebrafish by means of gross observations, pathological and transcriptome analysis. After BAPN administration, larval zebrafish showed changes in the form of periarterial hemorrhage, scoliosis, disruption of arterial ductal detachment and a resulting enlarged heart (Figure 1C). These results are similar to the toaortic phenotype sought by the gene mutation model constructed in Prendergast's laboratory (Andrew Prendergast et al. 2022). A 28% widening of the dorsal aorta after induction (statistically significant $P < 0.05$, as shown in Figure 1A and B) as well as the development of aortic arch malformations with a rate of 75% (6/8) (Figure 1C), is significantly correlated with the development of AAD (Shao-Qing Kuang et al. 2016; Mary B Sheppard et al. 2023). In the adult models, we found zebrafish treated with 1 mM BAPN for 22 days developed symptoms replicating the AAD pathological changes according to the Pathological Evaluation of AAD-like Alterations Table (Table S1; Cosmin Marian Banceu et al. 2023). Significant differences were observed in vessel diameter, vessel wall thickness, and degree of elastic fiber damage compared with controls ($P < 0.05$). Notably, the difference in aortic cross-sectional area was up to 2.46-fold ($P < 0.009$; Figure 2E), which is in line with the established human criteria for assessing aneurysms in patients (Jianing Gao et al. 2023). The normal vascular structure was disrupted and the vessel wall was significantly thickened in the modeling group ($8.22 \pm 2.23 \mu\text{M}$ vs. $26.38 \pm 10.74 \mu\text{M}$, $P < 0.05$; Figure 2F). Dilated dorsal aorta was shown to be associated with a decreased smooth muscle contractile phenotype. qPCR verified decreased mRNA levels of contraction-related genes in *cnn1a*, *cnn1b*, *acta2*, and *tagln* ($P < 0.05$). Transcriptome sequencing similarly revealed a significant decrease in genes and pathways associated with the smooth muscle contraction phenotype after BAPN modeling, with a shift to a smooth muscle synthetic phenotype. The enriched KEGG was consistent with the analysis of clinical patient samples collected in the laboratory of Erik Biros (Erik Biros et al. 2014), further validating the feasibility of the BAPN-induced zebrafish model.

Multiple lines of evidence suggested that the BAPN immersion can efficiently induce AAD formation in zebrafish. Both larval and adult fish have their own advantages. For example, short experimental time, simple procedures, simple observation techniques and cost-effectiveness are advantages of using larval zebrafish. However, it is unable to replicate specific

symptoms observed in human patients. A well-described hallmark of AAD in patients is the rupture of elastic fibers in the peritubular media (Jennifer P Habashi et al. 2006; Mark E Lindsay et al. 2012), which cannot be observed in larval fish because elastic fibers do not develop until after 5 dpf. The adult zebrafish AAD model offers another advantages, such as: pathological and molecular changes in adult zebrafish are very similar to those in human patients. In addition, the system exhibits remarkable stability, making it less susceptible to external influences. Further, imaging methods could be combined to assess the vascularity and blood flow changes.

4. Conclusion

BAPN induced a syndrome that resembles human AAD, including dorsal aortic widening and aortic arch deformity in larval zebrafish, and AAD-like pathological and molecular changes in adult zebrafish. Our results confirmed that zebrafish can be used as a viable animal for AAD modeling.

5. Materials and methods

5.1 Zebrafish

Tg[flk:EGFP] zebrafish, derived from AB/AB strain, (<http://zfin.org/ZDB-FISH-150901-14755>), were maintained in our lab following the protocols established by the National Zebrafish Resource Center. Prior to the experiment, six healthy transgenic zebrafish lines were carefully chosen on the afternoon preceding the experiment, one hour after their feeding. Male and female zebrafish were placed in a mating tank, separated into partitions. The following morning at 9:00 am, the partition was removed, allowing the male and female fish to engage in unrestricted mating for a duration of 0.5 h. Embryos were promptly collected within 10 min following spawning, and only the robust embryos were selected for grouping and subsequent administration. Following administration, the embryos were transferred to a culture dish and incubated in a controlled environment at 28.5°C.

Adult zebrafish were raised and bred following the guidelines and recommendations of the National Resource Center. The indoor temperature was maintained at 26°C ± 1°C, with a photoperiod of 14 h of light per day and a pH range of 7.0–8.0.

5.2 Modeling and imaging of larval zebrafish

After 2 h of embryo production, the embryos were evenly divided into a control group and a BAPN

(50 µM, MedChemExpress) treatment group, with 50 embryos in each group. BAPN was diluted in Holt buffer (NaCl 3.5 g/L, CaCl₂ 0.1 g/L, KCl 0.05 g/L, NaHCO₃ 0.2 g/L). After 72 h of induction, the subject was anesthetized and fixed on methylcellulose, and observed under a Stemi 508 stereo microscope. The dorsal aorta was observed and documented using an Axio Observer A1 fluorescence inverted microscope (Carl Zeiss).

5.3 Administration and ultrasound photography of adult zebrafish

3-month-old adult zebrafish were selected and their body length and weight were measured after tetracaine anesthesia. They were randomly divided into a control group and a BAPN group. The drug was administered for a total of 22 days, with the solution being replaced every three days with freshly prepared solution.

After administration, the zebrafish was placed into a plastic cup containing 100 ml of 168 µg/ml MS-222 (Fluka Analytical) for anesthesia. Following anesthesia, it was securely fixed onto a Vevo 3100 small animal ultrasound stand equipped with a 70 MHz ultrasound transducer for precise observation and photography purposes.

5.4 Dissection of dorsal aorta and RNA extraction

Adult zebrafish were anesthetized in standard embryo medium containing 168 µg/ml tricaine (ethyl 3-aminobenzoate methanesulfonate, MS222; Sigma). Their dorsal aorta, BA (Bulbus arteriosus) and OFT, were carefully dissected using fine forceps and micro scissors (Fine Science Tools) and placed in cold 1×PBS. After collection of three dorsal aorta per biological replicate, they were centrifuged at 4°C for 5 min at 16,873 g before being resuspended in TRIzol Reagent (Thermo Fisher Scientific) and flash frozen in liquid nitrogen. Total RNA was extracted from the tissues using Trizol (Invitrogen, Carlsbad, CA, USA) according to manual instruction and flash frozen in liquid nitrogen.

5.5 Real-time reverse transcription polymerase chain reaction (RT-qPCR)

Total RNAs were reverse transcribed into the first-strand cDNA using cDNA Synthesis Kit (Yeasen). The expression levels of mRNA were analyzed by real-time quantitative RT-PCR using the validated primers in iQ SYBR Green Supermix reagent kit (Bio Rad) on the StepOne Plus real-time system (Life Technologies). The relative mRNA levels were determined using the comparative

cycle threshold method, with β -Actin as the internal reference. The primers used are listed below.

acta2-FP:5'-AGAGGAACACCCCACTCTGT-3';

acta2-RP:5'-GTCCAGCACAATGCCTGTTG-3'.

tagln-FP:5'-AGCATCGCAGTCACCAAAGA-3';

tagln-RP:5'-TCACGTTCTTGCCCTCCTTC-3'.

cnn1a-FP:5'-ACAGGACGAACACTTGCAGA-3';

cnn1a-RP:5'-CACCAATGGCTCGCACAAG-3'.

cnn1b-FP:5'-TGGACATGGAGATGTGCGAC-3';

cnn1b-RP:5'-TATTCATTGGCGCTGGAGCA-3'.

actb-FP:5'-AGGAGAAGCTGTGCTACGTG-3';

actb-RP:5'-CCATACCCAGGAAGGAAGGC-3'.

5.7 Pathological analysis

To calculate the incidence of AAD in adult zebrafish, we adopted the presence of AAD-related pathological changes in the dorsal aorta as the standard. Following the removal of the head and tail, the zebrafish were divided into three sections, each averaging 3 mm. These sections were embedded together, and 500 μ M slices were cut, resulting in a total of five pieces (Figure S2 A).

Using the pathological scoring table from the Cosmin Marian Banceu laboratory, we graded the zebrafish slices. Each occurrence of indicators in the slices was recorded as a score. A comparison was then made between the two groups to determine whether the modeling group had indeed undergone AAD-like changes.

5.8 Statistical analysis

In this study, multiple comparisons were determined by one-way ANOVA, followed by Tukey's post hoc test. Conversely, in one comparison, the *p*-value was determined by unpaired two-tailed Student's *t*-test, two-tailed Welch's *t*-test, or two-tailed or single-tailed Fisher exact test. *p* < 0.05 was noted as statistically significant. The data is presented as mean \pm standard error (SE) or standard deviation (SD).

Ethical statement

All animal experiments were approved by the Institutional Animal Care and Use Committee of Guangdong

Provincial People's Hospital, by approval number S2022-010-01.

Acknowledgements

We sincerely thank Shanhai Biological Co., Ltd. for providing the Zebrafish breeding environment, and thank Dr. Azizullah Noor for his modification of the article format.

Disclosure statement

No potential conflict of interest was reported by the author(s).

Funding

This study was supported by grants from the National Natural Science Foundation of China [grant numbers 82272246 and 82072225 to Xin Li]; Science and Technology Program of Guangzhou, China [grant number 202206010044 to Xin Li]; High-level Hospital Construction Project of Guangdong Provincial People's Hospital [grant number DFJHBF202104 to Xin Li].

Author contributions

Xin Li, Haishan Zhao and Zhuoheng Lin conceived the idea, designed the study, and wrote the manuscript. JiariuiZhang performed the experiments, analyzed the data and wrote the manuscript. Yaowen Liang and Weiyue Zeng collected data and preparing experimental reagents. Xiaoyan Gao, DingchenWang and Cong Mai provided technical supports.

ORCID

Jiariui Zhang  <http://orcid.org/0009-0005-1666-8632>

Yaowen Liang  <http://orcid.org/0009-0006-1233-7964>

Weiyue Zeng  <http://orcid.org/0009-0006-4210-5582>

Xiaoyan Gao  <http://orcid.org/0000-0003-1172-4648>

Dingchen Wang  <http://orcid.org/0009-0008-1730-7363>

Cong Mai  <http://orcid.org/0000-0001-9287-866X>

Haishan Zhao  <http://orcid.org/0000-0001-7355-4627>

Xin Li  <http://orcid.org/0000-0003-0469-5121>

References

- Abrial M, Basu S, Huang M, Butty V, Schwertner A, Jeffrey S, Jordan D, Burns CE, Burns CG. 2022. Latent TGF- β binding proteins 1 and 3 protect the larval zebrafish outflow tract from aneurysmal dilatation. *Dis Model Mech.* 15(3): dmm046979. doi:10.1242/dmm.046979.
- Bahrami N, Childs SJ. 2020. Development of vascular regulation in the zebrafish embryo. *Development.* 147(10): dev183061. doi:10.1242/dev.183061.
- Banceu CM, Gurzu S, Satala C-B, Ghiga D, Neamtu MH, Voth V, Liebrich M, Suci H. 2023. Histopathological gap in aortic diseases: a prospective analysis. *Int J Mol Sci.* 24(20):15470. doi:10.3390/ijms242015470.

- Biros E, Moran CS, Rush CM, Gäbel G, Schreurs C, Lindeman JHN, Walker PJ, Nataatmadja M, West M, Holdt LM, et al. 2014. Differential gene expression in the proximal neck of human abdominal aortic aneurysm. *Atherosclerosis*. 233(1):211–218. doi:10.1016/j.atherosclerosis.2013.12.017.
- Chen T, Jiang N, Zhang S, Chen Q, Guo Z. 2021. BAPN-induced rodent model of aortic dissecting aneurysm and related complications. *J Thorac Dis*. 13(6):3643–3651. doi:10.21037/jtd-21-605.
- Gao J, Cao H, Hu G, Wu Y, Xu Y, Cui H, Lu HS, Zheng L. 2023. The mechanism and therapy of aortic aneurysms. *Signal Transduct Target Ther*. 8(1):55. doi:10.1038/s41392-023-01325-7.
- Gut P, Reischauer S, Stainier DYR, Arnaout R. 2017. Little fish, big data: zebrafish as a model for cardiovascular and metabolic disease. *Physiol Rev*. 97(3):889–938. doi:10.1152/physrev.00038.2016.
- Habashi JP, Judge DP, Holm TM, Cohn RD, Loeys BL, Cooper TK, Myers L, Klein EC, Liu G, Calvi C, et al. 2006. Losartan, an AT1 antagonist, prevents aortic aneurysm in a mouse model of Marfan syndrome. *Science*. 312(5770):117–121. doi:10.1126/science.1124287.
- Han J, Zhang R, Zhang X, Dong J, Chen M, Pan Y, Liao Z, Zhong M, He J, Wang F, et al. 2021. Zebrafish model for screening antiatherosclerosis drugs. *Oxid Med Cell Longev*. 2021:9995401. doi: 10.1155/2021/9995401.
- Hoareau M, Kholi NE, Debret R, Lambert E. 2022. Zebrafish as a model to study vascular elastic fibers and associated pathologies. *Int J Mol Sci*. 23(4):2102. doi:10.3390/ijms23042102.
- Kim HW, Stansfield BK. 2017. Genetic and epigenetic regulation of aortic aneurysms. *Biomed Res Int*. 2017:7268521. doi: 10.1155/2017/7268521.
- Kuang S-Q, Medina-Martinez O, Guo D-C, Gong L, Regalado ES, Reynolds CL, Boileau C, Jondeau G, Prakash SK, Kwartler CS, et al. 2016. FOXE3 mutations predispose to thoracic aortic aneurysms and dissections. *J Clin Invest*. 126(3):948–961. doi:10.1172/JCI83778.
- Levene CI. 1962. Studies on the model of action of lathyrogenic compounds. *J Exp Med*. 116(2):119–130. doi:10.1084/jem.116.2.119.
- Li J, Pan C, Zhang S, Spin JM, Deng A, Leung LLK, Dalman RL, Tsao PS, Snyder M. 2018. Decoding the genomics of abdominal aortic aneurysm. *Cell*. 174(6):1361–1372. doi:10.1016/j.cell.2018.07.021.
- Lin Y, Hu J, Xu R, Wu S, Ma F, Liu H, Xie Y, Li X. 2023. Application of logistic regression and artificial intelligence in the risk prediction of acute aortic dissection rupture. *Journal of Clinical Medicine*. 12(1):179. doi:10.3390/jcm12010179.
- Lindsay ME, Schepers D, Bolar NA, Doyle JJ, Gallo E, Fert-Bober J, Kempers MJE, Fishman EK, Chen Y, Myers L, et al. 2012. Loss-of-function mutations in TGFB2 cause a syndromic presentation of thoracic aortic aneurysm. *Nat. Genet*. 44(8):922–927. doi:10.1038/ng.2349.
- Nienaber CA, Clough RE, Sakalihan N, Suzuki T, Gibbs R, Mussa F, Jenkins MP, Thompson MM, Evangelista A, Yeh JS, et al. 2016. Aortic dissection. *Nat Rev Dis Primers*. 2:16053. doi:10.1038/nrdp.2016.53.
- Peterson RT, Macrae CA. 2012. Systematic approaches to toxicology in the zebrafish. *Annu Rev Pharmacol Toxicol*. 52:433–453. doi:10.1146/annurev-pharmtox-010611-134751.
- Powell JT, Brady AR. 2004. Detection, management, and prospects for the medical treatment of small abdominal aortic aneurysms. *Arterioscler Thromb Vasc Biol*. 24(2):241–245. doi:10.1161/01.ATV.0000106016.13624.4a.
- Prendergast A, Ziganshin BA, Papanikolaou D, Zafar MA, Nicoli S, Mukherjee S, Elefteriades JA. 2022. Phenotyping zebrafish mutant models to assess candidate genes associated with aortic aneurysm. *Genes (Basel)*. 13(1):123. doi:10.3390/genes13010123.
- Shannon AH, Culler JM, Dahl JJ, Scott EJ, Tyerman Z, Spinosa MD, Montgomery WG, Johnston WF, et al. 2019. Porcine model of infrarenal abdominal aortic aneurysm. *J Vis Exp*.(153). doi:10.3791/60169.
- Sheppard MB, Smith JD, Bergmann LL, Famulski JK. 2023. Novel SMAD3 variant identified in a patient with familial aortopathy modeled using a zebrafish embryo assay. *Front Cardiovasc Med*. 10:1103784. doi:10.3389/fcvm.2023.1103784.
- Stoletov K, Fang L, Choi S-H, Hartvigsen K, Hansen LF, Hall C, Pattison J, Juliano J, Miller ER, Almazan F, et al. 2009. Vascular lipid accumulation, lipoprotein oxidation, and macrophage lipid uptake in hypercholesterolemic zebrafish. *Circ Res*. 104(8):952–960. doi:10.1161/CIRCRESAHA.108.189803.
- Yang K, Ren J, Li X, Wang Z, Xue L, Cui S, Sang W, Xu T, Zhang J, Yu J, et al. 2020. Prevention of aortic dissection and aneurysm via an ALDH2-mediated switch in vascular smooth muscle cell phenotype. *Eur Heart J*. 41(26):2442–2453. doi:10.1093/eurheartj/ehaa352.
- Zheng H-Q, Rong J-B, Ye F-M, Xu Y-C, Lu HS, Wang J-A. 2020. Induction of thoracic aortic dissection: a mini-review of β -aminopropionitrile-related mouse models. *J Zhejiang Univ Sci B*. 21(8):603–610. doi:10.1631/jzus.B2000022.
- Zhou Y, Wang T, Fan H, Liu S, Teng X, Shao L, Shen Z. 2024. Research progress on the pathogenesis of aortic aneurysm and dissection in metabolism. *Curr Probl Cardiol*. 49(1 Pt A):102040. doi:10.1016/j.cpcardiol.2023.102040.